

FIRST RESULTS FROM THE ARECIBO GALACTIC HI SURVEY: THE DISK/HALO INTERFACE REGION IN THE OUTER GALAXY

SNEŽANA STANIMIROVIĆ¹, MARY PUTMAN², CARL HEILES¹, JOSHUA E. G. PEEK¹, PAUL F. GOLDSMITH^{3,4}, BON-CHUL KOO⁵, MARKO KRČO³, JAE-JOON LEE⁵, JEFF MOCK⁶, ERIK MULLER⁷, JAGADHEEP D. PANDIAN³, AARON PARSONS⁶, YVONNE TANG³, DAN WERTHIMER⁶

To appear in The Astrophysical Journal

ABSTRACT

The consortium for Galactic studies with the Arecibo L-band Feed Array (ALFA) is conducting a neutral hydrogen (HI) survey of the whole Arecibo sky (declination range from -1° to 38°), with high angular ($3.5'$) and velocity resolution (0.2 km s^{-1}). The precursor observations with ALFA of a region in the Galactic anti-center reveal numerous isolated, small (a few pc in size), and cold ($T_k < 400 \text{ K}$) HI clouds at low negative velocities, distinctly separated from the HI disk emission ('low-velocity clouds', LVCs). These clouds are most likely located in the transition region between the Galactic disk and halo (at scale heights of 60–900 pc), yet they have properties of typical cold neutral clouds. LVCs are colder and, most likely, smaller and less massive than Lockman's clouds in the disk/halo interface region of the inner Galaxy. Our observations demonstrate that the cloudy structure of the interface region is most likely a general phenomenon, not restricted to the inner Galaxy. LVCs have sizes and radial velocities in agreement with the expectations for clouds formed in low-temperature fountain flows, although we measure a factor of ten higher HI column densities. Alternatively, LVCs could represent the final stages of the infalling intergalactic material in the on-going construction of the Galaxy.

In the same dataset at higher negative velocities, we have discovered a 'companion' HI cloud located $50'$ southwest of CHVC186+19-114. CHVC186+19-114 is a typical compact high velocity cloud (HVC) with a well-defined core/envelope structure. The companion cloud has a diameter of only $7' \times 9'$, and is one of the smallest HVCs known, most likely stripped from the main cloud through the interactions with the halo medium.

Subject headings: ISM: clouds — ISM: structure — Galaxy: formation — Galaxy: halo — intergalactic medium

1. INTRODUCTION

The Galactic halo, a hot, ubiquitous multi-phase gas, with a low density, and temperature around 10^6 K , that surrounds our Galaxy is crucial to Galactic activity. As well as acting as a thermal insulator, the halo constrains models of the interstellar medium (ISM) in the Galactic disk through its impact on the dynamics of the hot intercloud component. From the theoretical point of view, the Galactic fountain model (Shapiro & Field 1976) was the first to address interactions between the disk and the halo. In this model, the hot gas flows from the disk into the halo, starts to cool, and falls back onto the disk. One of the later models, so called chimney model of the ISM (Norman & Ikeuchi 1989), suggested that the disk and the halo are connected through chimneys – large conduits resulting from superbubbles bursting out of the disk and forming collimated structures that can reach heights of $\sim 1 \text{ kpc}$. From the observational point of view, numerous ISM structures (shells, superbubbles, worms, chimneys, plumes) were found in the vertical gas distribution of our own Galaxy and several nearby galaxies, and have been postulated to play an important role in the transfer

of mass and energy between galactic disks and their halos. However, the details of how these structures replenish the hot halo gas are still not fully understood (Dove et al. 2000).

In understanding the ways in which the Galactic disk and halo are related the transition region between the Galactic thin disk and the halo, also known as the Galactic thick disk, is of special interest. This region extends to heights up to 1–1.5 kpc above the plane. The disk/halo interface region was discovered several decades ago (Shane 1967; Lindblad 1967) and was considered to represent a smooth envelope of neutral hydrogen (HI) surrounding the Galactic spiral structure. Further studies (Albert 1983; Danly 1989; Lockman 1986) found occasional isolated halo clouds at lower heights and suggested that this component could be pervasive, yet patchy, and most likely dynamically connected with the disk.

Galactic fountain and chimney models, as well as recent numerical simulations (de Avillez 2000), predicted the existence of small-scale, cloudy structure in the interface region, with clouds ranging in size from a few parsecs to tens or hundreds of parsecs. Recent observations with the

¹ Radio Astronomy Lab, UC Berkeley, 601 Campbell Hall, Berkeley, CA 94720 sstanimi@astro.berkeley.edu

² University of Michigan, Department of Astronomy, 500 Church St., Ann Arbor, MI 48109; mputman@umich.edu

³ Department of Astronomy, Cornell University, Ithaca, NY 14853

⁴ Jet Propulsion Laboratory, 4800 Oak Grove Drive, Pasadena CA 91109

⁵ Department of Physics and Astronomy, Seoul National University, Seoul 151-742, Korea

⁶ Space Sciences Laboratory, University of California, Berkeley, CA 94720

⁷ CSIRO Australia Telescope National Facility, PO Box 76, Epping, NSW 1710, Australia

Green Bank telescope (Lockman 2002) have actually revealed dramatic small-scale structure of the interface region in the inner Galaxy, composed of numerous discrete HI clouds. While this confirms the expectations from theoretical models and simulations, the full extent and the origin of this cloudy component is still not understood.

Another set of attractive questions concerning the disk/halo interface region comes from the idea that the formation of galaxies is an ongoing process (Oort 1966) and that the accretion of intergalactic material (IGM) serves as the main source of new star formation fuel (Maller & Bullock 2004; Murali et al. 2002). However, the details of the transformation from the smooth and hot IGM on kpc scales, down to clumpy and cold gas on star-forming scales, still need to be worked out. For example, what is the internal structure of IGM clouds at different stages of their infall? As searches for accretion remnants around other galaxies are difficult due to sensitivity and area limitations (e.g., Fraternali et al. 2002), our own Galaxy is still one of the best places to start seeking answers to these questions.

HI clouds in the Galactic halo at heights > 1 kpc have been studied observationally for several decades and are often classified into several distinct groups based on how much their velocities deviate from Galactic rotation (intermediate and high velocity clouds, HVCs), and their relative size (compact and extended clouds). Velocities reach approximate $+/- 450$ km s $^{-1}$ in the LSR reference frame and their sizes vary from over 100 deg 2 to compact HVCs with sizes of 4–30 arcmin (Putman et al. 2002; Brüns & Westmeier 2004). In addition, almost all HVCs, especially the more compact ones, clearly show head/tail or core/envelope structures, with heads or cores having a narrow linewidth while tails and envelopes having a significantly broader velocity structure, possibly showing signs of interaction with the ambient medium (e.g. Brüns & Mebold 2004). It is still not clear whether this range of observational properties, especially the low-end of the cloud size and velocity distributions, is caused by observational limitations. What determines the size and morphology of the observed halo clouds? Are these remnants of very different physical processes, or do different ‘types’ of clouds represent different stages of the same phenomenon — accretion onto the Galaxy, for example?

The questions above are just a subset of issues that still await to be addressed. The main purpose of this paper is to summarize the ongoing observational efforts to understand the properties of gas clouds from the halo to the plane by studying the disk/halo interface of our Galaxy. This work is inspired and enabled by the new multi-beam system, very recently installed at the Arecibo telescope⁸, which allows sensitive, large-scale HI surveys with an angular resolution of $3.5'$. Previous large-scale surveys of the link between the disk and the halo have been limited by resolution (Leiden-Dwingeloo Survey, $36'$; Hartmann & Burton (1997)), or an inability to trace features from the halo into Galactic emission (Putman et al. 2002). Recent high-resolution Galactic Plane surveys (Taylor et al. 2003; McClure-Griffiths et al. 2005) have been limited to trac-

ing the lower velocity and latitude HI emission and thus also do not provide adequate information on the disk/halo interface.

The structure of this paper is organized as follows. We start in Section 2 by briefly introducing the consortium for Galactic studies with the Arecibo L-band Feed Array (GALFA) and emphasizing the importance of the Arecibo telescope for large-scale Galactic surveys. Section 3 describes the observing strategy adopted for Galactic HI spectral-line surveys with ALFA. In particular, the fast scanning mode utilizing the basket-weave technique, and a newly developed method for obtaining reference HI spectra by multiple frequency switching, are applicable to radio telescopes in general. In Section 4 we summarize major previous observational studies of HI in the Galactic anticenter. We then present our results in Sections 5 and 6, and provide extensive discussion of observational and theoretical issues in Sections 7 and 9. We summarize our results and point out future studies in Section 10.

2. GALFA — BACKGROUND AND FUTURE

GALFA is a worldwide consortium of scientists (currently with 86 members) interested in undertaking large-scale Galactic surveys with the Arecibo L-band Feed Array⁹ (ALFA). GALFA members have been working together with the National Astronomy and Ionosphere Center in planning and executing large surveys to ensure their long-reached usage and availability by the greater astronomical community. The consortium consists of three sub-consortia for spectroscopic HI, radio recombination line, and continuum surveys. It is anticipated that data products from GALFA surveys will be archived and easily accessible by the astronomical community.

Galactic surveys with ALFA have greatly improved angular resolution in comparison with previous large-scale single-dish surveys. For example, the all-sky HI survey by Bell Laboratories (Stark et al. 1992) had angular resolution of 2° , while the HI all-sky survey with the Dwingeloo radio telescope (LDS; Hartmann & Burton 1997) had angular resolution of 0.6° . GALFA’s angular resolution of only $3.5'$ will be especially appreciated at high Galactic latitudes where high resolution, interferometric observations are still rare. At lower latitudes several recent, high resolution, surveys of the Galactic plane exist, or are underway (Taylor et al. 2003; McClure-Griffiths et al. 2005), with a typical angular resolution of $1-2'$ and a brightness sensitivity of $1.5-3$ K (per 0.8 km s $^{-1}$ wide velocity channels). To provide complete information about the large-scale HI structure these surveys combine data from interferometer and single dish telescopes.

The Arecibo telescope has several unique advantages over all other radio telescopes: (i) its unmatched collecting area, together with a large gain and low-noise receivers, results in an excellent and unrivaled filled surface-brightness sensitivity; (ii) this is the only radio telescope that can *simultaneously* provide both an high angular resolution, usually provided exclusively with interferometers, and a continuous range of spatial scales (including the largest scales, or so-called zero spacings), usually provided only

⁸ The Arecibo Observatory is part of the National Astronomy and Ionosphere Center, operated by Cornell University under a cooperative agreement with the National Science Foundation.

⁹ <http://www.naic.edu/alfa/>

with single dish telescopes. This unique combination of high surface-brightness sensitivity and accurate mapping of all angular scales above $3.5'$ makes the Arecibo telescope extremely valuable for Galactic science. In addition, ALFA, a cluster of seven receivers, has increased Arecibo's surveying (mapping) speed by a factor of seven, making the telescope a vastly more efficient system for covering large areas than an interferometer/single dish combination (Dickey 2002). In the fastest mapping mode commonly used for GALFA projects, the mapping speed is ~ 9.4 square degrees per hour. This results in a rms brightness sensitivity per beam of 0.1 K (per 0.72 km s^{-1} wide channels and after averaging both polarizations). For a spectral feature with a FWHM of $10\text{--}20\text{ km s}^{-1}$ our minimum ($3\text{-}\sigma$) detectable HI column density is $(5\text{--}11)\times 10^{18}\text{ cm}^{-2}$.

This paper focuses on only one of major science drivers for GALFA — the Galactic disk/halo interface region. The whole science case for Galactic HI spectral-line surveys is rich and diverse, full description can be found in the GALFA White Paper¹⁰. In addition, there are several projects planned for continuum and radio recombination line surveys which will be presented elsewhere. Currently, several different scientific HI projects are underway, some focusing on relatively limited areas of the sky (for studying, for example, particular molecular clouds and their possible connection with atomic gas), while some others requiring the coverage of the whole sky visible from Arecibo (the study of halo cloud properties, for example). The general survey philosophy has been to start with smaller, scientifically interesting regions, apply exactly the same observing parameters (velocity resolution, scanning mode etc.), and eventually combine all observations to build the whole “jigsaw puzzle” of the Galactic HI sky observable from Arecibo (declination range -1° to 38°).

While large-scale Galactic HI surveys with ALFA will address numerous outstanding questions regarding Galactic science, their importance for other scientific areas is also large. For example, X-ray observations need to be corrected for Galactic absorption using HI column density measurements. The small-scale structure ($< 30'$) in the neutral Galactic layer can alter significantly interpretation of X-ray data and needs to be accounted for (Bregman et al. 2003; Lockman 2004). Also, for the interpretation of UV absorption spectra, HI emission spectra with as high angular resolution as possible, approximating a pencil-beam toward a background source, are necessary (Wakker et al. 2003).

The large-scale HI Galactic survey with ALFA started in early 2005. Prior to this, in September–November 2004, short precursor observations were undertaken to test the instrumentation, observing techniques, and data reduction tools. One of those test runs focused on a region of interest for studies of the Galactic disk/halo interface region, in the Galactic anti-center, well known to harbor a wealth of high velocity gas. As a demonstration of the quality of HI images obtained with ALFA we present here observations of this region and preliminary results.

3. GALFA OBSERVATIONS AND DATA PROCESSING

The observations presented in this paper were undertaken in October and November of 2004, as a precursor observing run of the GALFA Consortium with the newly installed ALFA system. Our main aim was testing of the newly developed spectrometer (GALSPECT) and the proposed observing strategy. ALFA was installed at the Arecibo telescope in April 2004.

ALFA is a cluster of seven state-of-the-art dual polarization receivers operating at the frequency range $1225\text{--}1525\text{ MHz}$. ALFA was constructed at the Australia Telescope National Facility. Each of seven beams has a slightly elliptical shape, with the observed FWHM being relatively constant at $3.13' \times 3.57'$ (in Az and za) (Heiles 2004a¹¹; Deshpande et al. in preparation). The on-axis gain is 10.7 K Jy^{-1} for the central beam and $8.3, 8.5, 7.8, 8.3, 8.7$ and 8.3 K Jy^{-1} for the outer six beams, respectively (Heiles 2004b¹²). The beam efficiency (with the first sidelobe) ranges from 0.80 for the central beam, to $0.69\text{--}0.77$ for the outer beams. The observed beam properties agree very well with the theoretical predictions by Cortés-Medellin (2002). The central beam has the smallest and the most circularly symmetric sidelobe; the outer beams have asymmetric sidelobes.

3.1. GALSPECT

GALSPECT is a dedicated spectrometer for Galactic HI surveys. This newly developed FPGA-based system was specifically designed for GALFA's needs. GALSPECT takes simultaneously two spectra: a *science spectrum* covering 7.14 MHz with 8192 frequency channels, resulting in the fixed velocity resolution of 0.18 km s^{-1} , and a *calibration spectrum* covering 100 MHz with 512 frequency channels. The usable velocity range after data processing is -700 to 700 km s^{-1} .

GALSPECT performs the frequency analysis by means of a polyphase filter bank (Crochiere & Rabiner 1983). This is an extension of the segmented-FFT technique (Romney 1995) which improves greatly the channel separation (down to -80 dB) at a small increase in computational complexity (less than a factor of two). This means that there is essentially no ‘spectral leakage’, which results in superb interference isolation. The data are digitized using 8-bit A/D converters. With this many bits, the clipping correction is small and we do not apply it.

3.2. Observing strategy

The adopted observing strategy takes advantage of the basket-weave (or meridian-nodding) scanning. We observe always at the meridian by driving the telescope only in zenith angle. Each day a single basket-weave scan is completed. As the Earth rotates a scan draws a zigzag pattern in the RA–Dec coordinate frame. On consecutive days we obtain adjacent scans, shifted by $\sim 1.79'$, covering eventually the whole region of interest. To cover the region about $30^\circ \times 5^\circ$ in size that is presented in this paper, we required $2\text{ hours} \times 8\text{ days}$. The basket-weave scanning technique has been commonly used in the past for all-sky

¹⁰ http://www.naic.edu/alfa/galfa/galfa_docs.shtml

¹¹ <http://www.naic.edu/alfa/memos/>

¹² <http://www.naic.edu/alfa/memos/>

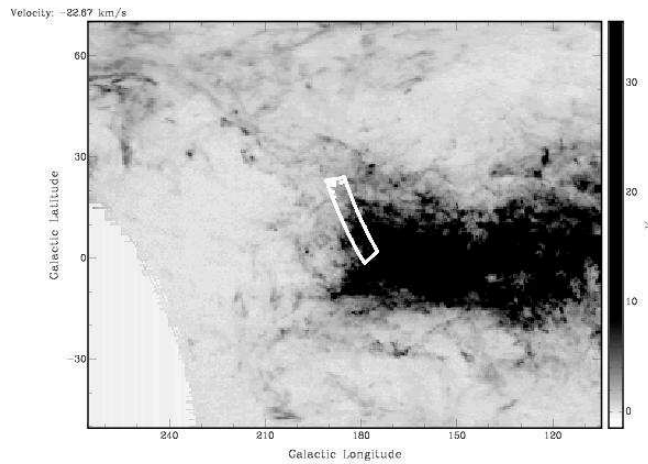


FIG. 1.— An image of the Galactic anti-center region from the Leiden-Dwingello survey (Hartmann & Burton 1997), at the LSR velocity of -22.67 km s^{-1} , emphasizing the filamentary structure seen at intermediate velocities. The white box outlines the region covered in GALFA’s precursor observations.

continuum surveys (for example see Haslam et al. 1982). It has several important advantages when imaging large areas of the sky: fast coverage of a large area of the sky, the beams always have the same orientation, inter-woven scans have many crossing points that allow a fine gain adjustment, and transit observations limit contamination from position-dependent sidelobes (which at Arecibo can be significant). This very fast observing mode scans the sky at a rate ~ 5.7 times faster than the sidereal rate, but covers every piece of the sky twice. The resulting integration time is 2.45 sec for each Nyquist pixel ($1.8' \times 1.8'$ in size). The separation between ALFA beams is $\sim 1.79'$ on the sky, close to Nyquist sampling, and it does not depend on the scanning speed. Practical details are given in the “GALFA HI User’s Guide”, Krčo et al. (2006)¹³.

Obtaining reference spectra is one large challenge GALFA HI surveys have to deal with. While mapping large-scale Galactic structure it is impossible to find an ‘empty’ point on the sky that will serve as a reference position. Commonly, the frequency switching technique is used when performing large-scale Galactic surveys. However, at many single-dish radio telescopes, and especially at the Arecibo telescope, the classic frequency switching technique introduces baseline problems because of frequency structure in the baseline produced by reflections. We have developed a new technique for obtaining a reference spectrum, called “The Least-Squares Frequency Switching” (LSFS, Heiles 2005a¹⁴). This technique derives the IF bandpass correction from a set of observations obtained with 7 LO frequencies. At the beginning and end of each day’s basket-weave scan we spend about 10 minutes to obtain LSFS data. The LSFS technique is based on cycling among 7 different LO frequencies and using the least-squares technique to separate the IF gain from the RF

spectrum. LSFS is performed separately on the 100-MHz calibration spectrum and on the 7.14-MHz science spectrum. Broad frequency structure in the IF bandpass and baseline of the science spectrum are derived from those portions of the calibration spectrum that lie outside the science spectrum’s band, and appropriate corrections are applied to the science spectrum.

3.3. Data reduction

A special purpose suite of IDL programs has been developed for the reduction of GALFA HI data, primarily by C. Heiles and J. Peek. The data reduction consists of five stages: bandpass correction, temperature calibration, cross-point correlation, fixed pattern noise reduction, and gridding. During the first stage, spectra from all beams are corrected for the IF gain, using the baseline as derived from the wideband calibration spectrum. We also correct here for a fast ripple that arises from reflections in the optical fiber that connects the control room with the feed cabin.

In the second stage of data reduction, spectra from all beams are calibrated into antenna temperature units using a fiducial conversion factor, which is later greatly refined. After this, crossing points of all beams are found in the data (this is typically a large number $\sim 420/\cos(\text{Dec})$ per square degree), crossing spectra are compared and the relative point-to-point gain corrections are determined. At the fourth stage, baselines of the beams are partially corrected for the fixed pattern noise (Heiles 2005¹⁵) using a beam-averaging process.

Finally, the last stage of data reduction includes gridding of calibrated and gain-corrected spectra from all scans into a spectral-line data cube. We use a program that assumes a Gaussian convolving kernel. Prior to gridding all

¹³ http://www.naic.edu/alfa/galfa/galfa_docs.shtml

¹⁴ http://www.naic.edu/alfa/galfa/galfa_docs.shtml#obs_data

¹⁵ <http://www.naic.edu/alfa/memos/>

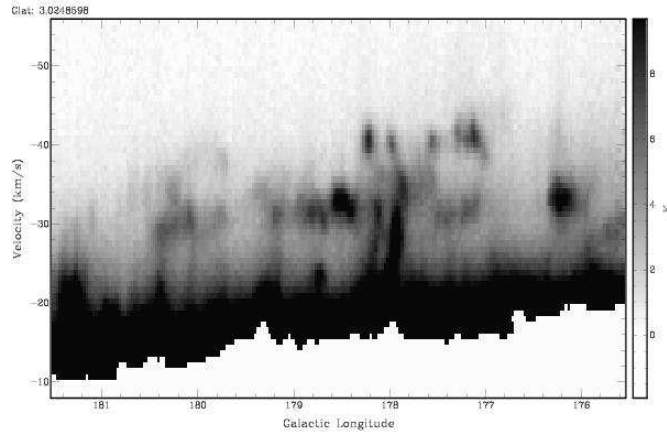


FIG. 2.— An example of interesting structure found in the anti-center data cube: cloudy structure at $b = 3^\circ$. A chimney-like extension is noticeable around $l \sim 178^\circ$ which may be connected with numerous small clouds at the velocity of $\sim -40 \text{ km s}^{-1}$. To enhance weak features all pixels with $T_B > 30 \text{ K}$ have been masked out.

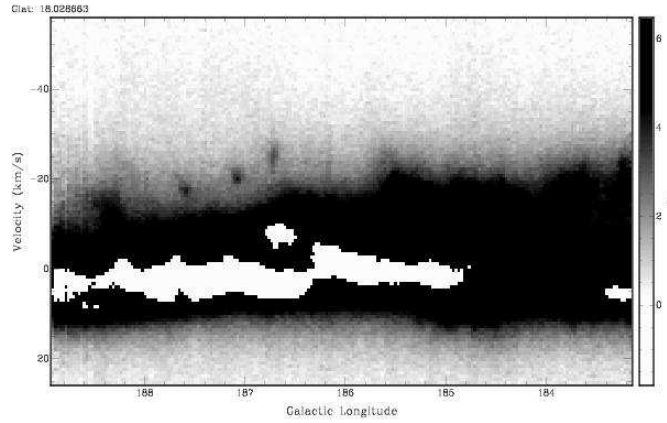


FIG. 3.— An example of interesting structure found in the anti-center data cube: three remarkable small HI clouds at $b = 18^\circ$, $l = 186\text{--}188^\circ$, at the LSR velocity -21 km s^{-1} . All pixels with $T_B > 12 \text{ K}$ have been masked out.

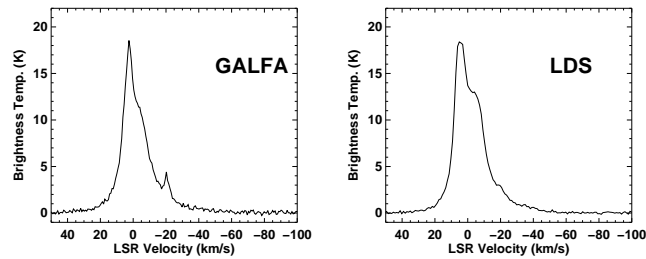


FIG. 4.— An HI velocity profile for the low-velocity cloud at $(l, b) = (187^\circ, 18^\circ)$ as obtained with GALFA and from the LDS data. This is the middle cloud seen in Figure 3. These profiles clearly demonstrate that the visibility of emission from a small feature at a velocity of -20 km s^{-1} is dramatically improved by a factor of 100 smaller beam solid area achieved by GALFA.

data are organized in a sparse matrix form which provides a memory-effective way of addressing a huge amount of data in IDL. The final post-gridding angular resolution is $3.5'$. In this particular data cube, a $1\text{-}\sigma$ noise level is 0.16 K , per 0.74 km s^{-1} wide velocity channel. The final data cube was at the end absolute-calibrated to match the brightness temperature scale of the LDS data for this region. To achieve this we scaled all spectra by a constant factor of 0.84.

3.4. Effects of stray radiation

The stray radiation properties of the Arecibo telescope are not well measured and understood. Above, we gave the main-beam plus first-sidelobe efficiencies; these vary from ~ 0.7 to 0.8 , which leaves a substantial residual beam response from sidelobes. A major question is: do these sidelobes reside at large angles from the main beam — normally referred to as “stray radiation” — as they do for smaller telescopes having significant blockage from structures like feed legs, or are they more concentrated toward the viewing direction?

We have performed some rough tests to examine this question. We compared emission profiles obtained in the Millennium survey (Heiles & Troland 2003a) with the LDS data, which are corrected for most effects of stray radiation. For data taken at modest zenith angles, below $\sim 17^\circ$, the Arecibo and LDS profiles have similar shapes in the line wings, where the effects of stray radiation are most noticeable. Moreover, our comparison of Millennium survey profiles of the same position taken at different times of year shows excellent agreement. The absence of significant response at large angles from beam center can be understood physically: most of the blockage at Arecibo is produced by structures that are much larger than a wavelength, so their diffraction patterns tend to be concentrated in a fairly tight angle around the beam center.

However, for pointing directions having zenith angle $\gtrsim 17^\circ$, the agreement between LDS and Arecibo profiles is not so good. Thus, for such directions, stray radiation at Arecibo does contribute artifacts in the line wings. This division line near zenith angle 17° makes sense because above that zenith angle the feed illumination pattern falls beyond the edge of the spherical primary reflector and onto the surface shield placed around its rim (so called skirt), which by its very nature produces far-out sidelobes with the consequent stray radiation. A project for the future is to pursue the measurement of this stray radiation in more detail.

Given this position-dependent stray radiation, we must ask how significant it is for our desired science. The attractive feature of mapping HI with the Arecibo telescope is the good angular resolution, compared to the LDS, combined with the high surface brightness sensitivity. Stray radiation has essentially no scientific impact on this attractive feature. The telescope’s stray radiation response comes from weak sidelobes that cover large angles in the sky, and these cannot produce structure on angular scales measured below a few degrees. In short, changes in the measured HI profile on angular scales of a few degrees cannot possibly be produced by the convolution of these weak, broad sidelobes with structure on the sky because even for a point-source sky feature the convolution produces a re-

sponse that has the angular scale of the sidelobes.

We conclude that on scales below of a few degrees, angular *structure*—i.e., *change* in the HI profile—is not affected by distant sidelobes. However, on the same scales the overall shape of our profiles are sometimes susceptible to contamination by stray radiation. These overall shapes need to be corrected by referring to a stray-radiation-corrected HI survey, of which the best is the Leiden-Argentine-Bonn (LAB) survey (Kalberla et al. 2005a; Hartmann & Burton 1997; Bajaja et al. 2005; Arnal et al. 2000). This survey has $\sim 36'$ resolution, and when our maps cover a reasonable area of a few square degrees we can correct our profiles by using this survey as a standard. We have not yet implemented such a correction procedure.

4. HISTORY OF STUDIES OF ANOMALOUS GAS IN THE ANTI-CENTER REGION

As mentioned in Section 2, the first GALFA observations focused on a region in the Galactic anti-center. The Galactic anti-center is well known as a region with a large amount of gas at forbidden velocities and hence offers the perfect case-study for Galactic disk/halo interfaces. Weaver (1970) was the first to point out interesting high-velocity, jet-like features in the Galactic anti-center region which were apparent at some longitudes and appeared to be connected to the low-velocity gas in the Galaxy. Several authors have studied these features further, for the full list of references please see Tamanaha (1997).

The most prominent structure in the anti-center region is the Anti-center Shell (ACS), discovered by Heiles (1984), and studied by several authors. This large supershell, with an angular diameter of almost $45^\circ \times 25^\circ$, is moving very fast (velocity $> 70\text{ km s}^{-1}$). However it appears to have stopped expanding. Several authors, including Kulkarni et al. (1985), have favored the explanation that the ACS was formed by an impact of a chain of high velocity clouds onto the Galactic disk. Tamanaha (1994) pointed out that the ACS has a wealth of filamentary structure at intermediate velocities, -25 to -90 km s^{-1} . By using a special filtering technique he was able to isolate seven filaments and propose a model in which filaments are located on the surface of a sphere with a radius of about 25° , centered on $l = 185^\circ$, $b = 0^\circ$. These filaments are large, having a typical length of $10^\circ\text{--}40^\circ$, and appear at mostly constant longitudes, and have typically FWHM of $10\text{--}20\text{ km s}^{-1}$. The chain of HVCs in the anti-center region, often referred to as clouds ACI, ACII etc., has been known for a long time. It is still unclear though whether these clouds are related to the ACS.

5. THE ANTI-CENTER FILAMENTS AND ‘COLD’ CLOUDS

This ‘pilot’ HI spectral-line data cube is centered on the Galactic anti-center region, $l \sim 180^\circ$, and covers a range of latitudes, $b = 0^\circ\text{--}23^\circ$, with $V_{\text{lsr}} = 90$ to -200 km s^{-1} . The original velocity resolution was 0.18 km s^{-1} , we have smoothed spectra by four channels resulting in the final velocity resolution of 0.74 km s^{-1} . In the velocity domain the data cube covers several distinctly different environments: Galactic HI, intermediate velocity gas at $V_{\text{lsr}} \sim -50\text{ km s}^{-1}$, a portion of the Outer Arm HVC complex at $V_{\text{lsr}} \sim -80\text{ km s}^{-1}$, and a typical compact high velocity cloud (CHVC) at $V_{\text{lsr}} \sim -115\text{ km s}^{-1}$. This

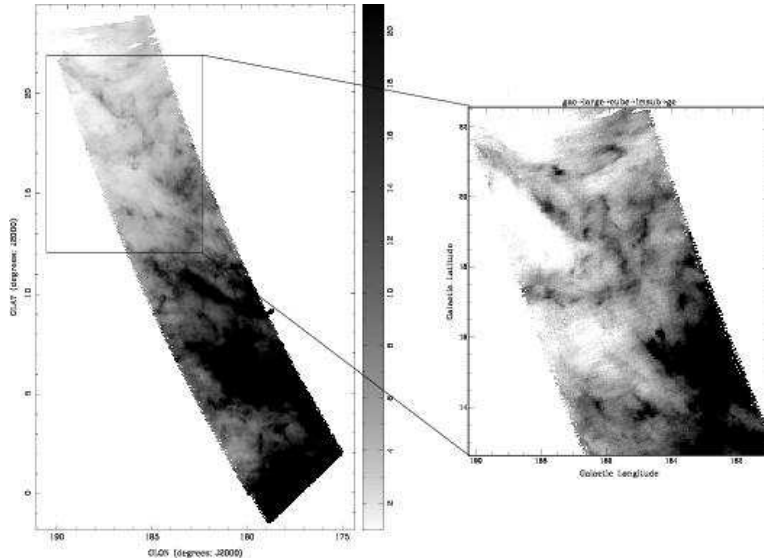


FIG. 5.— (left) An image obtained with ALFA showing filamentary structure at low forbidden velocities, around -22 km s^{-1} . The grey-scale range is 1 to 21 K with a square-root transfer function to enhance weak features. (right) A zoom in on the weak filamentary structure at $b \sim 18^\circ$ with a stretched intensity scale.

CHVC was cataloged as WvW215 by Wakker & van Woerden (1991) and as CHVC186+19-114 by Braun & Burton (1999).

Figure 1 shows a large view of the region, obtained from LDS. The white box included in this figure encloses the area covered in GALFA’s precursor observations. Our data offer one of the very first views of the high-latitude HI distribution at the high angular resolution of $\sim 3.5'$ with high surface brightness sensitivity. This view reveals several new and interesting phenomena, which we introduce in the following subsections. The compact HVC is introduced in Section 6.

5.1. Low-velocity clouds or LVCs

The region contains numerous discrete HI clouds at negative velocities of $V_{\text{lsr}} \sim -20$ to -40 km s^{-1} , shown in Figures 2 – 6. Throughout this paper we will call these clouds ‘low-velocity clouds’ (LVCs). Although LVCs are in the forbidden velocity range as the expected LSR velocity for gas in the Galactic anti-center and under Galactic rotation is $\sim 0 \text{ km s}^{-1}$, velocities up to 20 – 30 km s^{-1} are typically allowed to account for turbulent motions (Wakker 2001). Most of LVCs have $|V_{\text{lsr}}|$ slightly smaller than, or near the low velocity end of, what is traditionally assumed for intermediate velocity clouds (e.g. IVCs are defined as having $|V_{\text{lsr}}| \geq 30$ – 40 km s^{-1} ; Wakker 2001, Richter et al. 2003). Frequently, LVCs appear to kinematically follow the main Galactic disk structure.

This type of HI cloud is particularly common at the lower Galactic latitudes in our region. An example at $b = 3^\circ$ is shown in Figure 2, where numerous, discrete, narrow-linewidth HI clouds are easily noticeable. Some of these discrete clouds are connected in velocity to lower velocity gas; the strongest example is at $\ell = 178^\circ$. In this particular data cube HI clouds like these are not common at intermediate Galactic latitudes, $b \approx 7$ – 15° , while they become again very frequent at high latitudes, $b > 15^\circ$. Clouds at high Galactic latitudes are especially easy to notice, and most of them appear to be associated

with faint, diffuse filamentary structures.

A spectacular example of LVCs at $b = 18^\circ$ is shown in Figure 3: three small HI clouds (the smallest cloud has an angular size of only $4.5'$), with extremely narrow velocity linewidths ($\sim 2 \text{ km s}^{-1}$) are noticeable at distinctly different LSR velocities from those of the bulk HI disk emission. However, the clouds clearly follow the distribution of the disk HI with longitude, and are probably affected by the general Galactic rotation. Figure 4 shows spectra of one of the three clouds as obtained with GALFA (left panel) and from LDS (right panel). The LDS profile only barely hints at the -20 km s^{-1} feature, which is so prominent in the GALFA profile. Clearly these HI clouds are too small to be visible in low-resolution surveys and were missed.

5.2. Low-velocity filamentary structures

The region has prominent filamentary structures, especially near $V_{\text{lsr}} = -25 \text{ km s}^{-1}$ — covering roughly the same velocity range as that of the discrete clouds. These filaments are clear in Figure 5 (left), which shows a velocity channel at $V_{\text{lsr}} = -22.1 \text{ km s}^{-1}$. The filaments may be related to the larger filaments noted previously in the anti-center region and studied extensively by Tamanaha (1994, 1997); however the character of these filaments changes dramatically when viewed with our full angular resolution. Figure 5 (right) zooms in on the black square in the left panel. With this higher magnification, these filaments are peppered with numerous embedded HI clouds. Most of the clouds are small, $\sim 5'$ – $10'$ in size, and very difficult to notice in previous low-resolution HI images.

5.3. Cloud morphology

Several LVCs have especially interesting morphology suggestive of core/envelope structure which is indicative of the multi-phase medium. Figure 6 (left) shows an example of a possible connection between the disk HI and HI clouds at $V_{\text{lsr}} = -38$ and -50 km s^{-1} — two weak HI ‘bridges’ ($T_{\text{B}} \sim 1 \text{ K}$) are noticeable extending from the disk to the

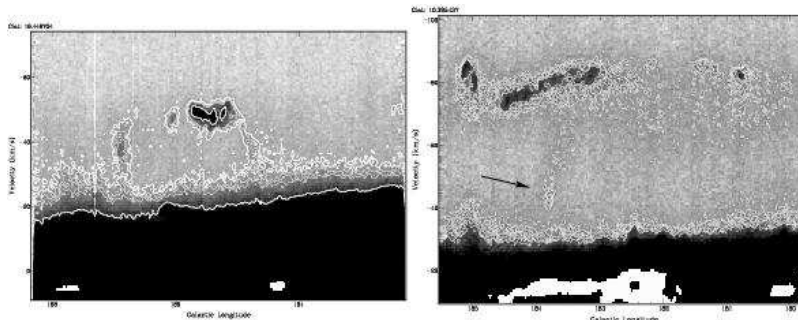


FIG. 6.— Two examples of interesting cloud morphologies found in the anti-center data cube. To enhance weak features all pixels with $T_B > 30$ K have been masked out. (left) An example of a larger cloud at $(l, b) = 186.9, 16.4^\circ$ at a velocity of -38 km s^{-1} which shows weak elongations (tails), with $T_B \sim 1$ K, at both lower and higher velocities. Similarly, the intermediate-velocity cloud at a velocity of -50 km s^{-1} has a tail ($T_B \sim 1\text{--}1.5$ K) connecting it with the disk HI emission. Contours are at 1.0, 1.25, 1.5 and 3.0 K. The grey-scale range is -2 to 12 K with a linear transfer function. (right) A cloud at $(l, b) = 183.8, 10.4^\circ$, at a velocity of -43 km s^{-1} which appears to have a weak tail trailing all the way to -80 km s^{-1} . Contours range from 5 (0.75 K) to $10\text{-}\sigma$ (1.5 K).

intermediate velocity gas, suggesting a possible physical connection. Both clouds and bridges could also represent segments of a larger, shell-like structure. There is no evidence, however, that the size of the shell-like feature changes systematically with latitude, as it would in the case of an expanding shell. The cloud $183.81+10.37$, indicated in Figure 6 (right) with the black arrow, is another interesting example — it has a faint ‘tail’ ($T_B \sim 1$ K) that trails toward the intermediate-velocity gas at $V_{\text{LSR}} \sim -80 \text{ km s}^{-1}$.

5.4. Properties of low-velocity clouds

To avoid confusion with Galactic emission we have selected a small set of 12 clouds with $b > 10^\circ$ which stand out as obvious, well-separated features. These clouds are distinct, well separated from the Galactic plane emission, and have negative deviation velocities $-42 < V_{\text{dev}} < -25 \text{ km s}^{-1}$. Wakker (2001) defined the deviation velocity as the minimum value of the deviation of the cloud’s radial velocity from Galactic rotation. In this framework, clouds with negative V_{LSR} and negative V_{dev} appear to be moving toward us too fast relative to what is allowed by Galactic rotation. This set of clouds is by no means complete. Our aim is to demonstrate the existence of small, cold HI clouds in the outer Galaxy, at forbidden velocities and most likely located in the Galactic disk/halo interface region, as well as to describe their basic properties. With a larger amount of collected data in the near future we will be able to do a statistically more meaningful analysis.

Figure 7 shows velocity profiles through the centers of selected HI clouds. HI clouds/condensations easily stand out as distinct peaks with a central velocity in the range ~ -25 to $\sim -42 \text{ km s}^{-1}$. To measure the clouds’ basic properties we have fitted each velocity profile with a few Gaussian functions. Results from this fitting procedure are summarized in Table 1 where we provide the range of: cloud angular sizes, V_{LSR} , velocity FWHM (Δv), the peak brightness temperature ($T_{B,\text{max}}$), and the peak HI column density ($N(\text{HI})_{\text{peak}}$). In Figure 8 central positions of selected clouds are shown with crosses on a $l - V_{\text{LSR}}$ image. Each pixel in this image represents the peak brightness temperature over the latitude range $b = 15^\circ\text{--}19^\circ$. This image depicts almost continuous extent of cloudy structure between the disk HI emission and the intermediate velocity

gas at $\sim -50 \text{ km s}^{-1}$. Many of LVCs appear to kinematically follow the disk HI, but 2–3 clouds with the most negative velocities could be related to the intermediate-velocity gas. Several small clouds at positive LSR velocities, around $+20 \text{ km s}^{-1}$, are also noticeable in this figure.

Most of LVCs must be very cold. The velocity FWHM for all 12 clouds is in the range $3.0\text{--}7.6 \text{ km s}^{-1}$. The mean FWHM is 4.4 km s^{-1} , and the mean $T_{k,\text{max}}$ (the kinetic temperature in the case there is no nonthermal broadening) is only 470 K. 80% of clouds in this (small) sample have $T_k < 450$ K and FWHM of $3\text{--}4 \text{ km s}^{-1}$. The clouds’ mean central LSR velocity is -33 km s^{-1} and the mean peak HI column density is $2 \times 10^{19} \text{ cm}^{-2}$. The cloud angular size ranges from $6'$ to $12'$. Here we focus only on well-isolated and compact clouds; but there are also clouds with diameters of up to $30'$ in the data cube which we will discuss in a future paper.

5.5. Properties of low-velocity filaments

Most of these clouds appear related to diffuse filamentary features (Figure 4) which are seen as broad line wings in the Galactic HI profile. From the fitting of velocity profiles as well as visual inspection, the filaments have a large FWHM, typically $20\text{--}30 \text{ km s}^{-1}$, and their peak brightness temperature is low, $T_B = 1\text{--}2$ K. Their sizes are of order of a few degrees, some filaments may extend beyond our maps. Typical HI column densities are $(4\text{--}12) \times 10^{19} \text{ cm}^{-2}$.

6. CHVC186+19-114

Figure 9 shows HI channel maps of CHVC186+19-114 which is present in the same data cube at higher negative velocities. The top ten panels in this figure show primarily a more diffuse, or envelope structure, having asymmetric, ring-like morphology. The same panels also show an interesting ‘companion’ HI cloud, seen for the first time in our observations, and located ~ 50 arcmin to the southwest of CHVC186+19-114. The more compact (core) component of this CHVC is primarily at higher negative velocities, typically between -115 and -122 km s^{-1} , and is visible in the remaining panels of Figure 9.

6.1. Properties of core/envelope structure

To obtain physical parameters of the HVC’s core and envelope separately, we have fitted each velocity profile with

TABLE 1
MEASURED PROPERTIES OF HI CLOUDS AND FILAMENTS AT LOW AND HIGH NEGATIVE VELOCITIES.

	Angular size (arcmin)	V_{lsr} (km s^{-1})	FWHM (km s^{-1})	$T_{\text{B,max}}$ (K)	$N(\text{HI})_{\text{peak}}$ (10^{19} cm^{-2})
Low-velocity clouds	6–12	–25 to –42	3.0–7.6	1.6–4.1	1–3
Low-velocity filaments	a few deg	–20 to –30	20–30	1–2	4–12
CHVC186+19-114 Core	30×40	–110 to –118	4–7	~ 1 –4	~ 1 –11
CHVC186+19-114 Envelope	30×65	–100 to –118	~ 16	0.5–1.5	3–13
CHVC186+19-114 Companion	8	–100 to –107	~ 15	0.8	6

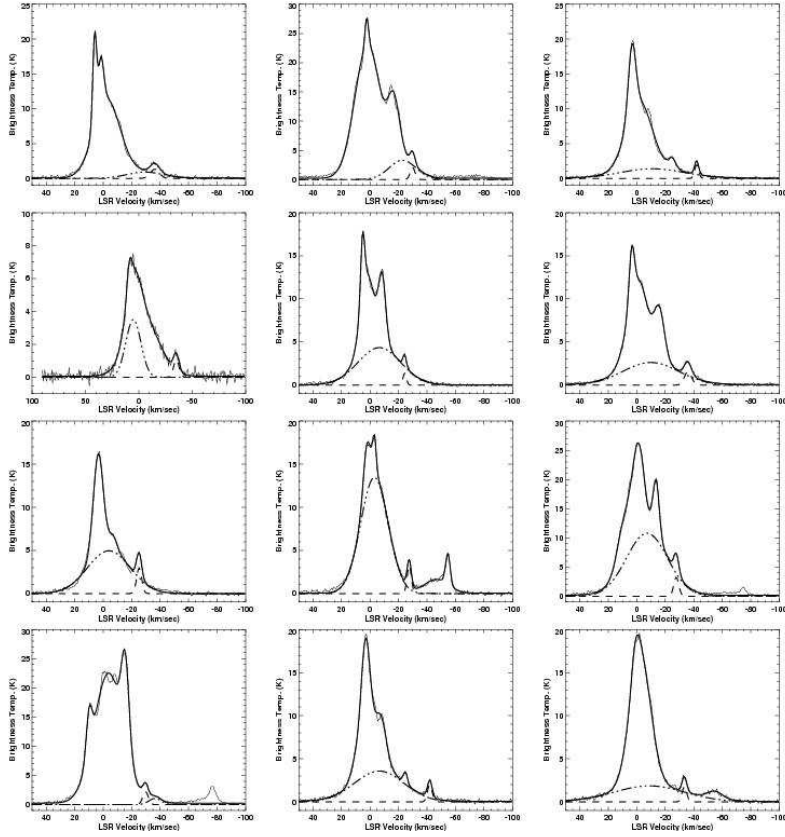


FIG. 7.— Velocity profiles of 12 small, isolated HI clouds. The thin solid line shows the data, the thick solid line is the combined best fit, the dashed line shows the Gaussian component corresponding to HI low-velocity clouds, and the dot-dashed line depicts a broad, diffuse component, which is almost always needed to produce a good fit.

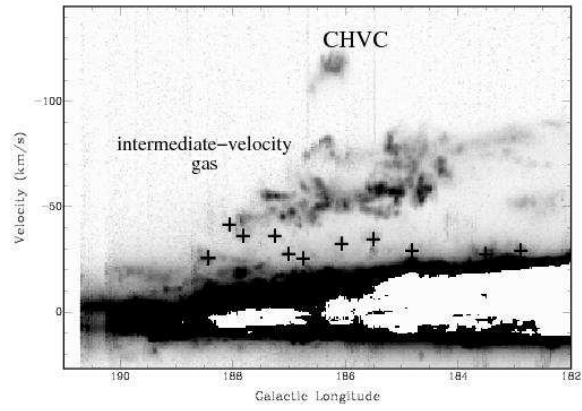


FIG. 8.— An HI peak brightness temperature image over the latitude range $b = 15^\circ$ to 19° . The grey-scale range is 0 to 17 K, with a linear transfer function; pixels with $T_B > 25$ K have been masked out to enhance weaker features. Crosses show central positions of selected clouds in our sample.

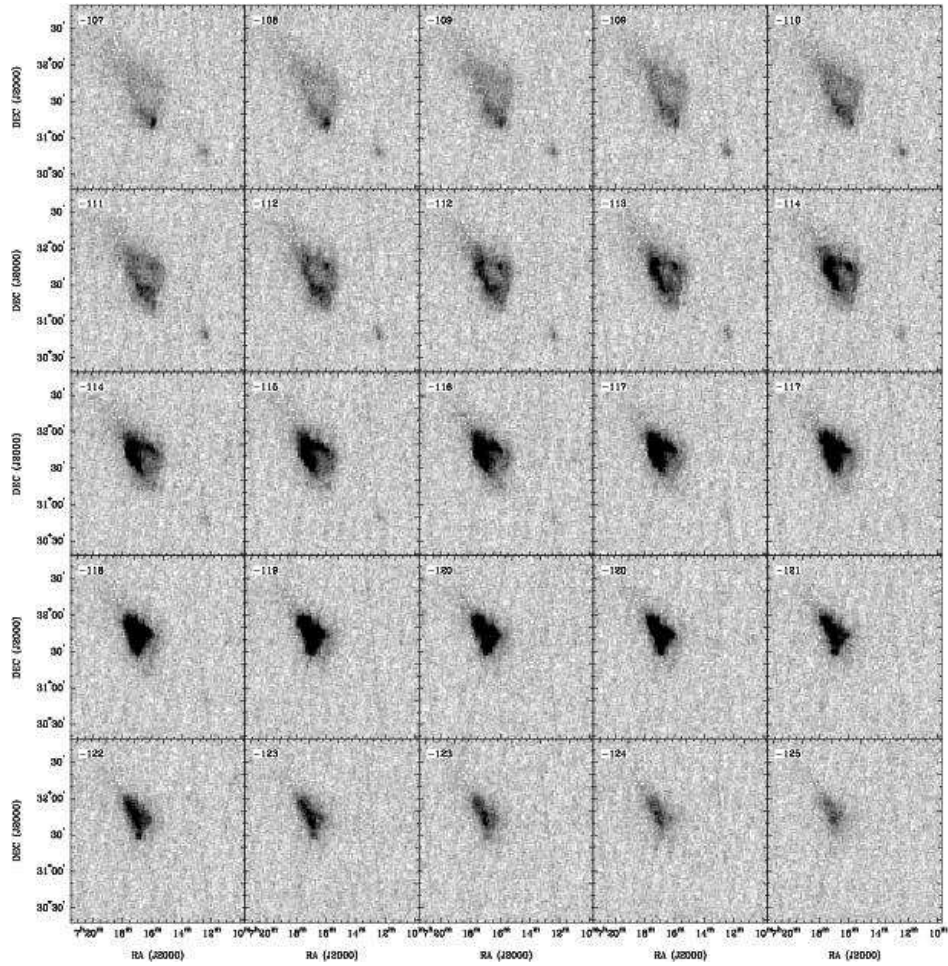


FIG. 9.— HI images of CHVC186+19-114 at the LSR velocities specified in the top-left corner of each panel. The grey-scale intensity range is -0.5 to 2 K with a linear transfer function.

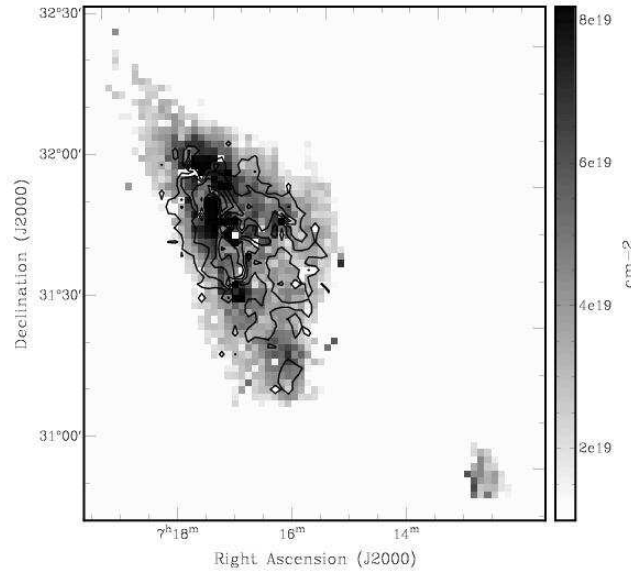


FIG. 10.— HI column density image of the broad velocity component shown in grey-scale. HI column density distribution of the narrow velocity component is shown with black contours. Contour levels range from 1×10^{19} to 1.1×10^{21} cm^{-2} , with a step of 2×10^{19} .

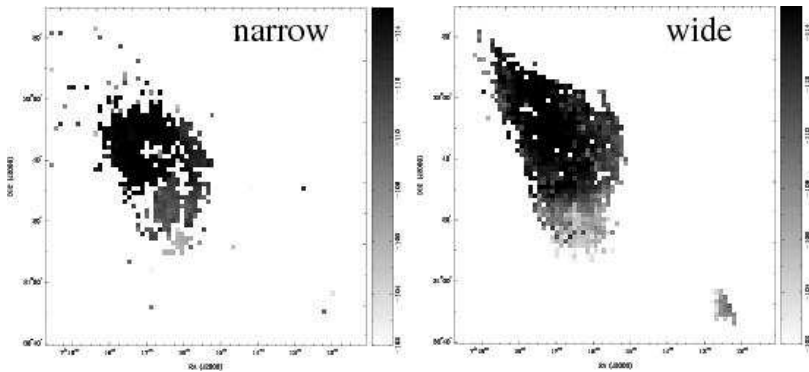


FIG. 11.— The velocity field of the narrow velocity component (left) and the wide velocity component (right).

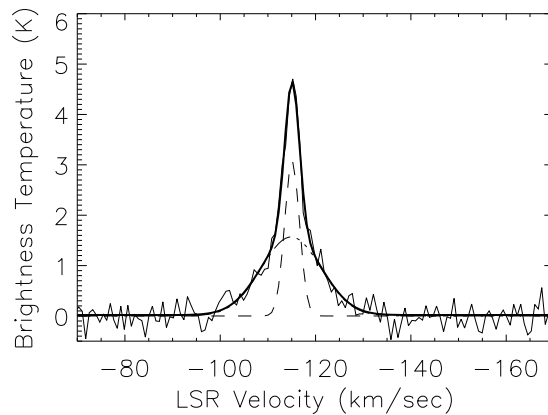


FIG. 12.— An example of extremely narrow velocity profiles found at several locations in CHVC186+19-114. This profile was obtained at RA $07^{\text{h}} 18^{\text{m}} 2.5^{\text{s}}$, Dec $31^{\circ} 44' 46.5''$ (J2000) and was fitted with two Gaussian functions: the narrow function has a FWHM of 3.7 km s^{-1} (shown with the dashed line), and the wide function has a FWHM of 14.7 km s^{-1} (shown with the dot-dashed line). The total fit is shown with the thick solid line.

one or two Gaussian functions. For this exercise, only pixels with a brightness temperature $T_B > 3\sigma$ were selected. Regions spatially corresponding to the core structure are typically well-fitted with a combination of one narrow and one wide Gaussian function. Most of the envelope, as well as the HI companion cloud, is well-fitted with a single, broad Gaussian function. Figure 10 shows HI column densities of the narrow (contours) and wide (grey-scale) Gaussian components, while their velocity fields are shown in Figure 11.

An interesting result is that both narrow and wide velocity components show a clear velocity gradient from ~ -104 km s $^{-1}$ in the south to ~ -118 km s $^{-1}$ at the north. This suggests that the same physical mechanisms affect and de-accelerate both cold and warm gas in this CHVC. The central LSR velocity of the companion cloud is -107 km s $^{-1}$, while its typical FWHM linewidth is ~ 18 km s $^{-1}$. The wide component has a typical FWHM linewidth of $\sim 15 - 18$ km s $^{-1}$, while the narrow component has a FWHM of ~ 7 km s $^{-1}$. Interestingly, there are several small regions in this CHVC where the narrow velocity component has much smaller linewidth. As an example Figure 12 shows a velocity profile where the colder component has a FWHM of only 3.7 km s $^{-1}$, indicative of cold gas with the kinetic temperature < 300 K. The narrow and wide velocity components of the main cloud have comparable peak $N(\text{HI})$ of $\sim 10^{20}$ cm $^{-2}$, while the companion cloud has a peak $N(\text{HI})$ of $\sim 5 \times 10^{19}$ cm $^{-2}$.

As mentioned earlier, the main cloud of CHVC186+19-114 was cataloged previously (Wakker & van Woerden 1991; Braun & Burton 1999) and also partially imaged at high resolution with the Arecibo telescope (Burton et al. 2001) and with the Westerbork Synthesis Radio Telescope (de Heij et al. 2002). Burton et al. (2001) found that CHVC186+19-114 has a core/envelope morphology and fitted its velocity profiles with two Gaussian functions. Based on the measured exponential $N(\text{HI})$ profile as a function of cloud’s radius, being interpreted as due to a spherical exponential distribution of the HI volume density distribution, Burton et al. (2001) estimated CHVC186+19-114’s distance to be 600–800 kpc. Maloney & Putman (2003), however, showed that exponential $N(\text{HI})$ profiles could be a natural consequence of an external source of ionizing photons and cannot be used to derive HVC’s distances. de Heij et al. (2002) noted a velocity offset between the CNM component, traced in interferometric data, and the WNM component, derived from the total power, Arecibo data. They suggested that this systematic offset could be explained by some type of external perturbations, one possibility being ram-pressure interactions with the external medium.

6.2. Relation of main and companion clouds

GALFA observations cover a significantly large area around CHVC186+19-114, revealing a ‘companion’ HI cloud. The companion cloud has the central LSR velocity very similar to that of CHVC186+19-114’s envelope and lags behind CHVC186+19-114’s core by ~ 10 km s $^{-1}$. In addition, velocity profiles (T_B and FWHM) on the south side of the HVC envelope are similar to profiles through the companion cloud. This is all suggestive of a possible physical association between CHVC186+19-114 and the

companion cloud. One possibility is that this small cloud has been stripped from CHVC186+19-114’s envelope due to ram pressure interactions with the halo medium. This cloud could represent an evidence for the break up of HVCs into smaller clouds due to ram pressure (or even tidal) interactions. Another possibility is that both CHVC186+19-114 and the companion cloud are embedded in lower column density gas and we are just able to detect the high column density peaks of this extended ‘complex’.

The companion HI cloud has an angular size of only $7' \times 9'$ and could be classified as one of the smallest HVCs ever detected. Its size is just at the lower end of the size distribution of the mini-HVC population discovered recently by Hoffman et al. (2004).

7. OBSERVATIONAL DISCUSSION: LOW-VELOCITY CLOUDS

7.1. Distances and HI masses of low-velocity clouds

A major unknown parameter of LVCs is their distance. As we have shown in Section 5.4, 80% of LVCs in our sample have $T_k < 400$ K and FWHM of only 3–4 km s $^{-1}$. The peak $N(\text{HI})$ for all clouds is $(1-3) \times 10^{19}$ cm $^{-2}$. These linewidths and column densities are very similar to those of ordinary CNM clouds at $|b| > 10^\circ$ studied through HI absorption measurements (Heiles & Troland 2003b), suggesting that the anti-center LVCs are likely to be ‘‘true’’ CNM clouds. As mentioned earlier, LVCs often appear related to larger, warmer filamentary structures, with a typical FWHM of 20-30 km s $^{-1}$.

In the Galaxy, the CNM and WNM can co-exist only over a certain, well-defined range of thermal pressures, P_{\min} to P_{\max} [this was first emphasized by Field et al. (1969) and most recently re-examined by Wolfire et al. (2003)]. This co-existence of cold LVCs with warm filamentary structures can be used to estimate cloud distances. As the ISM is highly turbulent, often turbulent pressure is more important than the thermal pressure. However, as nicely explained in Wolfire et al. (2003), on the scales of typical CNM clouds thermal pressure dominates, and CNM clouds are expected to be embedded in a spatially isobaric medium with their surface layers having the same thermal pressure as the ambient warm medium. Wolfire et al. (2003) calculated P_{\min} and P_{\max} in the Galactic midplane for several Galactocentric radii (R_g). Both quantities decrease with R_g . For example, at $R_g = 8.5$ kpc, $P_{\min} = 1960$ K cm $^{-3}$ and $P_{\max} = 4810$ K cm $^{-3}$, while at $R_g = 18$ kpc, $P_{\min} = 272$ K cm $^{-3}$ and $P_{\max} = 1220$ K cm $^{-3}$.

We can now calculate for our LVCs their volume density (n) and thermal pressure (P) using: $n \propto N(\text{HI})_{\text{peak}} \times D^{-1}$ and $P \propto nT_{k,\text{max}}$, where $T_{k,\text{max}} = 21.86\Delta v^2$. Both n and P depend on the cloud distance D , also these equations assume that clouds are spherically symmetric (please note that sheets will have higher pressure, while cigars oriented towards the observer will have lower pressure). Estimates for both $n \times D$ and $P \times D$ are given in Table 2, together with the estimated maximum kinetic temperature and the peak HI column density. We can now compare measured values for $P \times D$, for each cloud, with the thermal pressure allowed for the CNM and WNM co-existence to estimate D . If we assume the typical thermal pressure in the Solar neighborhood of 3000 K cm $^{-3}$, then clouds in our sample have the distance range 0.1–1.3 kpc, with the median

TABLE 2

DERIVED (MEDIAN) PROPERTIES OF HI CLOUDS AND FILAMENTS AT LOW AND HIGH NEGATIVE VELOCITIES.

	$T_{k,\max}$ (K)	$N(\text{HI})_{\text{peak}}$ (10^{19} cm^{-2})	$n \times D$ ($\text{cm}^{-3} \times \text{kpc}$)	$nT_{k,\max} \times D$ ($10^3 \text{ K cm}^{-3} \times \text{kpc}$)
Low-velocity Clouds	200–1300	1.0–3.0	1.3–5.5	0.3–4
Low-velocity Filaments	9000–20000	4–12	0.7–1.5	10–20
CHVC186+19-114 Core	350–1000	2–11	0.9	1
CHVC186+19-114 Envelope	5600	2–13	0.8	4
CHVC186+19-114 Companion	5000	5	3.2	16

distance being 0.3 kpc. The lowest thermal pressure that allows the CNM and the WNM to co-exist is $\sim 270 \text{ K cm}^{-3}$ (Wolfire et al. 2003), this places an upper limit on the distance to our clouds of $\sim 3.6 \text{ kpc}$ (this value is the median for the whole cloud sample). The highest thermal pressure that allows the CNM and the WNM to co-exist is $\sim 5000 \text{ K cm}^{-3}$ (for $R_g \gtrsim 8.5 \text{ kpc}$ as our clouds are in the direction of the Galactic anti-center), this places a lower limit on the distance to our clouds of $\sim 0.2 \text{ kpc}$. If the thermal pressure is, however, $> 5000 \text{ K cm}^{-3}$ then cloud distances could be $< 0.2 \text{ pc}$ and our clouds may be very closeby. Such high thermal pressures are not expected to be common in the Galaxy for $R_g > 8.5 \text{ kpc}$ from the theoretical point of view. If present they would indicate the existence of very short-lived, transient clouds. The observed morphology of LVCs, in the form of discrete, isolated clouds with sharp edges and appearing over many velocity channels, does not suggest their transient character. However, future direct distance measurements are essential to confirm cloud distances. We also caution that our distances were estimated under the assumption of the *local* pressure equilibrium at cloud surfaces. Several recent observations and numerical simulations have challenged the global pressure equilibrium condition for the interstellar gas, however still mildly favoring the local pressure equilibrium state (for example see Mac Low et al. 2005).

Table 2 also gives $P \times D$ for low-velocity filaments, which appear higher than for the clouds and are most likely due to a non-spherical, sheet-like morphology. This is supported by the visual appearance of filaments which have a far more elongated morphology than the clouds.

If we assume for now that the LVCs have distances in the range 0.2–3 kpc, then their height from the plane is in the range 60–900 pc. As the typically assumed scale height (half-thickness) of the Galactic thin disk is $z_{\text{thin}} = 100 \text{ pc}$ (Belfort & Crovisier 1984; Kulkarni & Heiles 1988; de Avillez 2000), most of the LVCs appear located in the transition region between the thin disk and the hot Galactic halo. With a typical angular radius of $9'$, LVCs' linear size is 0.5–8 pc, while their HI mass ranges from 3×10^{-2} to $7 M_{\odot}$. If the clouds are embedded in the warm medium with a temperature of 6000 K, then the mass-loss rate due to evaporation (calculated using eq. [47] in McKee & Cowie (1977)) is $1.5 \times 10^{24} \text{ gr yr}^{-1}$, and hence the cloud evaporation timescale is $\gtrsim 100 \text{ Myr}$.

Several previous observational studies have found cold clouds at significant heights above the disk in our own Galaxy and in several other spiral galaxies. Crawford et al. (2002) obtained NaI and CaII observations towards

the opening of the Local Interstellar Chimney and found cold neutral clouds with low negative velocities, located at $0.3 < |z| < 2.5 \text{ kpc}$. They suggested that these clouds most likely belong to a scattered population of infalling diffuse clouds, consistent with a Galactic Fountain model. Howk (2005) discussed evidence for cold, CNM-like, gas in the disk/halo transition region of several spiral galaxies based on optical imaging of extra-planar dust. They suggested that this gas was most likely expelled from the thin disk through a quiescent process. Richter et al. (2003) found evidence for H_2 in dense, mostly neutral phase, and closely linked to CNM clouds in IVCs at even higher z heights. These results support our distance estimate, however the formation mechanism(s) for cold clouds in the disk/halo transition regions remain under debate (see Section 9.1).

7.2. Is there a link between our low-velocity clouds and Lockman's clouds?

One of the most important results of this study is that GALFA observations clearly demonstrate the cloudy structure of the Galactic disk/halo interface region in the outer Galaxy. The cloudy disk/halo interface, emphasized recently by Lockman (2002) in the inner Galaxy, is obviously not restricted just to the inner Galaxy and could be quite extended radially. We compare here properties of the disk/halo interface clouds in the inner and outer Galaxy.

Recent HI observations with the Green Bank telescope showed that the halo in the inner Galaxy is not smooth but populated with discrete HI clouds (Lockman 2002). These clouds, often referred to as “Lockman's clouds”, are located $\sim 900 \text{ pc}$ below the plane. However, they appear to kinematically follow the HI distribution in the disk. We summarize typical properties of this cloud population in Table 3. Frequently, clouds are organized into larger structures and connected by diffuse envelopes and/or filaments which can have sizes up to $\sim 1 \text{ kpc}$. In addition, high resolution observations (Lockman & Pidopryhora 2004) show that most Lockman's clouds have significant sub-structure, suggestive of the presence of a two-phase medium.

Stil et al. (2005) discovered an additional set of 17 isolated HI clouds in the inner Galaxy, with velocities up to 60 km s^{-1} greater than the maximum velocity allowed by Galactic rotation (see Table 3). Despite their forbidden velocities, these clouds follow the main disk emission and therefore cannot be classified as high-velocity gas. Located within the Galactic thin disk, at $|z| \lesssim 80 \text{ pc}$, these fast-moving clouds demonstrate that interstellar clouds can have very large random velocities along the line-of-sight. Stil et al. (2005) suggested that the fast-moving clouds, at

TABLE 3
 MEDIAN PROPERTIES OF ‘DIFFERENT’ TYPES OF HI CLOUDS IN THE GALACTIC DISK/HALO INTERFACE REGION.

Reference	Number of clouds	l (°)	b (°)	V_{dev} (km s ⁻¹)	Size (pc)	FWHM (km s ⁻¹)	$N(\text{HI})_{\text{peak}}$ ($\times 10^{19}$ cm ⁻²)	D (kpc)	$ z $ (pc)	M_{HI} (M_{\odot})
Lockman (2002)	38	28–29	–4 to –12	15 to 40 ^a	24	12	2	7.5	950	$\lesssim 50$
Stil et al. (2005)	17	18–67	–1.3 to 1.3	25 to 60	$\sim 10^b$	6	20	8	80	60
This work	12	183–188	12 to 23	–25 to –40	0.5–8	4	2	0.2–3	60–900	0.03 – 7

^aOne half of clouds in this study has $V_{\text{dev}} \leq 15$ km s⁻¹. Median $V_{\text{dev}} = 13$ km s⁻¹.

^bMost of the clouds in this study appear significantly elongated.

$|z| \lesssim 80$ pc, and Lockman’s clouds, at $|z| \sim 950$ pc, may belong to the same population of clouds that is widely spread throughout the Galaxy. Both works focused exclusively on clouds at tangent points in the inner Galaxy and therefore have well-determined cloud distances.

Table 3 lists properties of LVCs in the outer Galaxy to facilitate their comparison with HI clouds in the inner Galaxy. This table gives: the number of clouds in each study, the range of Galactic longitude and latitude, cloud deviation velocities (as defined in Section 5.4), median linear sizes, FWHM, peak HI column densities, typical distances, heights above the plane, and estimated HI masses.

Several potentially important differences are noticeable.

(1) It is striking that our LVCs, which lie outside the Solar circle, are on average smaller, colder, and less massive than clouds in the inner Galaxy. For our selected sample, most clouds have FWHM of 3–4 km s⁻¹, a factor of three smaller than that of Lockman’s clouds. Angular sizes of LVCs are in the range 6’–12’ (with a few exceptional examples having a size of only 4’), while Lockman’s clouds have a median size of $\sim 11'$.

Linear sizes and HI masses of LVCs are of course uncertain as they depend on cloud distances. However distances of 6–8 kpc, which would bring HI masses close to those of Lockman’s clouds, would imply the thermal pressure of 100 K cm⁻³ which is below the minimum pressure at which the CNM can exist in thermal equilibrium (Wolfire et al. 2003). Cloud angular sizes in our study though could be partially a selection effect, as we have focussed on well-isolated compact clouds for which Lockman’s angular resolution is less adequate.

(2) $|V_{\text{dev}}|$ of LVCs is on average higher than that of Lockman’s clouds. The median deviation velocity for Lockman’s sample is 13 km s⁻¹, while LVCs have $\langle |V_{\text{dev}}| \rangle = 30$ km s⁻¹. If real, this difference could be important, suggesting that interface clouds at larger galactocentric radii (> 8 kpc) have larger deviation velocities than clouds at smaller radii ($\lesssim 5$ kpc). Again, the difference in $|V_{\text{dev}}|$ is at least partially due to our selection criterion — to avoid confusion with the disk emission we have selected clouds with $|V_{\text{dev}}| \gtrsim 25$ km s⁻¹, but clouds with lower $|V_{\text{dev}}|$ also exist in the data set. Larger cloud samples from the GALFA surveys will be able to clarify whether clouds with larger V_{dev} are more common in the outer Galaxy.

(3) It is also important to notice that LVCs have negative V_{dev} , meaning they are moving toward us at velocities too fast to be explained by the Galactic rotation. Lockman’s clouds, however, have systematically positive V_{dev} ,

meaning they are moving away from us with velocities too fast to be explained by the Galactic rotation.

In conclusion, if our clouds would have distances of 6–8 kpc then their properties would be similar to those of Lockman’s clouds, but this would imply the thermal pressure below what is traditionally allowed for the CNM. If, however, our clouds are at distances $\lesssim 2 - 3$ kpc, then they are colder, smaller, and less massive than Lockman’s clouds. Taking into account various selection effects and different resolution provided by the Arecibo and Green Bank telescopes, clouds in the inner and outer Galaxy may belong to the same population with a range of properties (z , sizes, HI masses). However, distinctly different formation mechanisms can not be excluded either at this stage. Halo clouds with sizes similar to those of our LVCs were reported recently by Kalberla et al. (2005b) and Dedes et al. (in preparation). Using the Effelsberg radio telescope these authors found about 20 HI clouds at $R_g = 13 - 17$ kpc and $z = 3 - 5$ kpc. However, when viewed at high resolution with the Very Large Array, these clouds resolve into smaller cores with a FWHM of 3–7 km s⁻¹, a peak HI column density of a few $\times 10^{19}$ cm⁻², and diameters of a few pc.

8. OBSERVATIONAL DISCUSSION: ULTRA-COMPACT HVCS

The CHVC studied in this paper, CHVC186+19-114, is fairly typical of the ~ 250 currently cataloged CHVCs with diameters generally on the order of 20’–80’ (Putman et al. 2002; de Heij et al. 2002). The resolution and sensitivity of GALFA observations offer an unique opportunity to detect a large number of newly identified ultra-compact HVCs (UCHVCs), or HVCs with diameters $\lesssim 20'$. The number of these UCHVCs that have been identified to date remains limited. The smallest was found by Brüns & Westmeier (2004) and has an angular size of 4.5’ and a peak HI column density of 2×10^{20} cm⁻² (Brüns & Westmeier 2004). Slightly larger UCHVCs ($> 9'$; referred to as mini-HVCs) were found by Hoffman et al. (2004) with much lower peak column densities ($< 10^{19}$ cm⁻²); a similar UCHVC was mapped by Richter et al. (2005). These UCHVCs have been completely missed in the lower resolution surveys and it remains unclear if they will follow the power law distribution of flux density, column density and size found for other HVCs, or if they represent a distinct population of objects.

The companion cloud in Figure 8 has a size of only 7’ \times 9’ and a linewidth of 18 km s⁻¹ and can thus be classified as one of the smallest HVCs known. These UCHVCs may

represent a variety of objects. They may be the breaking up of a large cloud as it is stripped via a combination of tidal and ram pressure forces. The UCHVCs may also represent high column density peaks in a mostly ionized or lower column density high-velocity complex. In this case the UCHVC may represent the beginnings of a halo cloud cooling out of the hot diffuse medium.

The close match between the position and velocity of the UCHVC and the CHVC in our data does indicate they are directly related. This is similar to the CHVCs in the vicinity of the Magellanic Stream that show a spatial and kinematic link to the main structure of the Stream (Putman et al. 2003; Brüns et al. 2005). Also, properties of the companion cloud (angular size and FWHM) are similar to those of HI condensations (cores) observed with the Westerbork Synthesis Radio Telescope in the case of CHVC120 – 20 – 443 (de Heij et al. 2002). CHVC120 – 20 – 443 is one of the only two known CHVCs with exceptionally broad linewidths in its CNM (core) condensations, and de Heij et al. (2002) suggest that it may be undergoing ram-pressure or tidal stripping. Finally it remains possible that the UCHVCs represent small dark matter halos as proposed for the CHVCs (Braun & Burton 1999). Future GALFA observations of larger areas on the sky will be important for establishing the spatial distribution and properties of UCHVCs.

9. DISCUSSION: THEORETICAL ISSUES

9.1. *Galactic Fountain and ballistic clouds*

One of the most common models for the interaction between the Galactic disk and the halo is based on Galactic fountain flows (Shapiro & Field 1976; Houck & Bregman 1990). In this model, hot gas from the disk is pushed up by the stellar activity in the form of buoyant outflows, it travels through the halo, cools down, and as a result of thermal instabilities rains back onto the disk in the form of cold clouds. In their best model for low-temperature fountains (model 3; for a halo temperature of 3×10^5 K and a volume density 10^{-3} cm^{-3}) Houck & Bregman (1990) suggested that about 70 cold halo clouds should be present above a disk area of 400 pc^2 , having a typical size of $\sim 3 \text{ pc}$, a temperature of 500 K, and a column density of $2.5 \times 10^{18} \text{ cm}^{-2}$. A peak in cloud distribution is expected at the location of cloud formation, $z \sim 1\text{--}2 \text{ kpc}$, however if drag is important then the density of clouds at $z < 0.5 \text{ kpc}$ could be significant too. The expected radial velocities for fountain clouds are in the range from $-100 \sin b$ to $+50 \sin b \text{ km s}^{-1}$. 3-D simulations of a Galactic fountain by de Avillez (2000) also show the formation of numerous small cloudlets, with sizes down to their resolution limit of 1.25 pc , resulting from a breakup of collimated structures and also larger clouds being swept up by blast waves.

Typical sizes of LVCs are surprisingly similar to what is expected for fountain clouds. In addition, at $b = 17^\circ$, the expected velocity range for fountain clouds is -30 to 15 km s^{-1} (note that clouds at the positive velocities would be very difficult to detect due to confusion with Galactic HI), again very much in agreement with what we find for LVCs. The observed $N(\text{HI})$ of LVCs is about ten times higher than what is expected for fountain clouds, although Houck & Bregman (1990) note that $N(\text{HI})$ could be higher if clouds are concentrated at lower z heights.

Another important evidence in favor of the fountain-style clouds is hinted by cloud deviation velocities. Collins et al. (2002) investigated a ballistic infall of fountain clouds and showed that a vertical velocity gradient (with scale height z) is expected for halo clouds; this is a consequence of a decrease in the gravitational acceleration vector with height from the disk. Hence, at any galactocentric radius, the LSR velocity of clouds in the Halo, at $z > 1 \text{ kpc}$, will be different from the LSR velocity of clouds in the disk. However, the steepness of this vertical velocity gradient is a function of the galactocentric radius at which clouds originated before being kicked upward from the disk. For example, for the input circular velocity of 230 km s^{-1} and at a galactocentric radius of $R_g = 8 \text{ kpc}$, the expected ΔV_{lsr} is $\lesssim 30 \text{ km s}^{-1}$ when z changes from $z = 0$ to $z \sim 2 \text{ kpc}$ (assuming an initial cloud kick velocity of 100 km s^{-1}). Note that viscous interactions between Halo clouds, and/or more complex interactions between the Halo medium and clouds can decrease ΔV_{lsr} . However, for very small galactocentric radii, $\Delta V_{\text{lsr}} \approx 0 \text{ km s}^{-1}$, for any z . The expected LSR velocity difference (ΔV_{lsr}) for clouds at higher z relative to clouds in the disk, is therefore something we can directly compare with the cloud deviation velocity, V_{dev} .

The anti-center LVCs have $\langle |V_{\text{dev}}| \rangle = 30 \text{ km s}^{-1}$, in agreement with what is expected for fountain clouds at heights $z = 1\text{--}2 \text{ kpc}$. The expected circulation timescale (time for clouds to return back to the disk) for the fountain clouds is about 50 Myr (Houck & Bregman 1990; Collins et al. 2002). As the cloud evaporation timescale ($\gtrsim 100 \text{ Myr}$) is significantly longer than the expected circulation timescale, clouds can reach the disk safely before being evaporated. In Section 7.2 we hinted at a potentially interesting difference in $|V_{\text{dev}}|$ for clouds in the inner and outer Galaxy — most halo clouds in the inner Galaxy appear to have smaller $|V_{\text{dev}}|$ than clouds in the outer Galaxy. This potential trend in $|V_{\text{dev}}|$ is an important tool for investigating cloud origin — if halo clouds are a result of a Galactic fountain we would expect $|V_{\text{dev}}|$ to increase with galactocentric radius. Future work with larger cloud samples will investigate statistical significance of this trend.

In conclusion, LVCs have typical linear sizes and radial velocities in good agreement with expectations from the Galactic fountain model. This would suggest that Galactic fountain flows, and the circulation of fountain clouds, are (at least) as common in the outer Galaxy as in the inner Galaxy. This is a surprising result when one takes into consideration that the Galactic star formation rate (SFR) strongly depends on galactocentric radius, based on various observations as well as predictions from chemical and spectrophotometric models for the evolution of spiral galaxies (for references see Boissier & Prantzos (1999) and Boissier et al. (2003)). The star formation rate peaks around $R_g \sim 4 \text{ kpc}$ and then steadily decreases towards larger radii, at $R_g \sim 12 \text{ kpc}$ for example, $\text{SFR} \sim 0.3 \times \text{SFR}_\odot$. However, the decrease in SFR at large radii is alleviated partially by the decrease of the gravitational potential which enables vertical fountain flows to propagate easier.

9.2. *Connection between filaments and clouds*

Most of LVCs appear related to large, diffuse HI filamentary features. Diffuse filaments and clouds both appear only over a restricted range of LSR velocities, -20 to -30 km s $^{-1}$. This is suggestive of their possible physical association.

An association between larger filaments and small, cold clouds is expected as a result of shell or chimney fragmentation. Norman & Ikeuchi (1989) expect that clouds formed from chimney walls will have velocities $|v| \sim 10\text{--}50$ km s $^{-1}$. McClure-Griffiths et al. (2006) found several cold HI clouds associated with caps of a large expanding shell and suggested that shell fragmentation is responsible for the cloud formation. Similarly, Koo et al. (2006) proposed that small, fast-moving clouds could be fragments of old supernova remnant shells.

Visual appearance of filaments and clouds (Figure 4) strikingly resembles recent numerical simulations by Audit & Hennebelle (2005) of dynamically triggered condensation of the WNM into small CNM clouds. In these simulations, a collision between incoming turbulent WNM streams creates a thermally unstable region of higher density and pressure but lower temperature, which starts to fragment into cold structures. This thermally unstable WNM has a filamentary morphology, and is seeded with numerous small (size of ~ 0.1 pc) and cold clouds ($n \sim 50$ cm $^{-3}$, $T \sim 80$ K). The whole process of fragmentation is promoted and controlled by turbulence, and cloud morphology and properties, as well as the fraction of the condensed cold gas, are governed by turbulent properties. Based on this apparent morphological similarity it may be reasonable to expect that external (dynamical) forcing (through, for example, collisions, or interactions with the dense halo gas) of some types of vertical WNM flows (e.g. chimneys or walls of expanding shells) can trigger condensation of warm HI into cold clouds.

9.3. *Infalling multi-phase gas?*

The idea that galaxies acquire their fresh star formation fuel through the infall of clouds has attracted a lot of attention, especially recently with advances in numerical simulations of galaxy formation (Maller & Bullock 2004). As the hot gas within the cooling radius (~ 150 kpc for the Milky Way size galaxy) is a subject to thermal instabilities, it fragments into smaller, warm ($T \sim 10^4$ K), pressure-supported clouds. The warm clouds fall into the Galaxy, after undergoing cloud-cloud collisions and ram pressure stripping, and are tidally broken into smaller clouds before impacting the Galaxy. The cloud formation and infall are expected to be balanced at the present time, and models predict abundant evidence for this ongoing process in the Galactic halo, in the form of numerous condensed clouds.

Kaufmann et al. (2006) investigate the formation of a galactic disk, through N-body and SPH simulations, and show that cloud accretion is not spherical but happens along the angular momentum axis. This results in outer disks preferentially being populated with small, cold accretion remnants, while the central regions below and above the plane channeling hot gas. In this scenario, cloudy structure of the disk/halo interface region is expected in the inner and outer galactic disks but due to a very different phenomenon — while outer parts are driven by the accretion process, the inner parts could be a result of a

fountain process.

However, what exactly happens to clouds during the final stages of their infall is still mainly unexplored, both theoretically and observationally. How do large and warm clouds transform into ‘cloud forms’ that can easily be integrated and digested by the disk, to provide a smooth build up of fresh star formation fuel? Maller & Bullock (2004) suggest that clouds get shredded into smaller but still warm ($\sim 10^4$ K) condensations, with further cooling being stopped by the extragalactic ionizing background. Clouds in outer disks in simulations by Kaufmann et al. (2006) are also warm, 100–600 pc in size, however apparently they can cool and condense further to reach thermal equilibrium at a temperature $< 10^4$ K.

CHVCs and our LVCs may be able to fit into this framework as representing later stages of the cloud infall process. CHVC186+19-114 shown in Figures 8–11, typical of several hundreds of compact HVCs, could represent a cloud that has condensed in the halo and has begun to infall, but has not yet reached the disk. The low-velocity filamentary/cloudy structure, shown in Figures 2–7, could represent the remaining structure of the accreted cloud as it is being almost integrated with the Galactic disk. This scenario seems plausible when one considers the similarities between these two types of objects (see Table 1): CHVC186+19-114’s ‘core’ structure has velocity linewidths and HI column densities comparable to those found in LVCs, while typical HI linewidths and column densities of the filamentary structures at about -25 km s $^{-1}$ are very similar to those of CHVC186+19-114’s envelope. If the LVCs trace the final stages of the infall process then they suggest cloud sizes and temperatures significantly smaller from what is currently found in numerical simulations. However, details of heating/cooling and self-shielding effects during the cloud infall still await to be addressed. Observationally, constraining metallicities of halo clouds would be the crucial test of the cloud infall hypothesis.

10. SUMMARY AND FUTURE WORK

The consortium for Galactic studies with ALFA is conducting an HI survey of the whole Arecibo sky (declination range from -1° to 38°) with high angular ($3.5'$) and velocity resolution (0.2 km s $^{-1}$). At the time this article is being written about 20% of the survey has already been completed. In this paper we focused only on one of the main science drivers for GALFA — the Galactic disk/halo interface region. With only about 200 square degrees imaged in the Galactic anti-center region, primarily for the purpose of hardware and software testing, several interesting and new phenomena have emerged.

We have found numerous small (most likely just a few pc in size) and cold ($T_k < 400$ K) HI clouds at low negative velocities distinctly separated from the HI disk emission (‘low-velocity clouds’ or LVCs). Over a restricted range of velocities and exactly the same range as for LVCs, we have also found larger sheet-like filamentary structures. Most likely, the LVCs and filaments are physically related. While the distances to LVCs will have to be better constrained in the future, preliminary estimates, based on the thermal pressure requirements for the CNM and the WNM coexistence, range from 0.2 to 3 kpc. This implies

that the clouds' height from the plane is in the range 60 to 900 pc, suggesting that most LVCs are located in the transition region between the Galactic disk and halo, yet they have properties of typical CNM clouds. LVCs are colder and, most likely, smaller and less massive than Lockman's clouds in the disk/halo interface region in the inner Galaxy. In addition, LVCs may have larger absolute deviation velocities than Lockman's clouds. Nevertheless, the existence of a large number of LVCs in the outer Galaxy (at a galactocentric radius > 8 kpc) demonstrates that the cloudy and frothy character of the interface region is more likely to be a general phenomenon, not restricted exclusively to the inner Galaxy.

In the same dataset but at more extreme negative velocities we have studied CHVC186+19-114, a typical CHVC with a well-defined core/envelope structure. As we have imaged a large area around the CHVC, we discovered a companion HI cloud located $50'$ southwest of CHVC186+19-114, most likely physically related to CHVC186+19-114. Velocity profiles suggest that the companion cloud was stripped off the main cloud's envelope due to the interactions with the halo medium. This is the first time that a companion is detected around an isolated CHVC and may represent evidence for the breakup of CHVCs into smaller condensations. Based on its size, the companion cloud could be classified as a member of the population of UCHVCs, discovered only very recently.

We have discussed briefly three possible scenarios for the formation and maintenance of the clumpy Galactic disk/halo interface region. The first scenario is provided by Galactic fountains, buoyant hot flows from the disk which cool and rain back in the form of cold clouds. Observational properties (cloud size and radial velocity) of LVCs are in a good agreement with predictions of low-temperature fountains models. The second scenario is motivated by numerical simulations by Audit & Hennebelle (2005) of dynamically triggered condensation of the WNM into small CNM clouds. Vertical WNM flows propagating upward from the Galactic plane, in the form of expanding shells or chimneys, could be triggered into formation of CNM clouds at larger z heights. This comparison is primarily based on morphological resemblance at this stage as detailed models do not exist. Finally, the third scenario investigates whether the low-velocity clouds/filaments could represent the final stages of the infalling IGM. This has

been encouraged by the recent models and simulations (Maller & Bullock 2004; Kaufmann et al. 2006) which emphasize the multi-phase and multi-scale character of the galaxy formation process. While simulations show encouraging qualitative resemblance at this stage the detailed physical processes during the final stages of cloud infall are largely unexplored. We hope that our current, and especially future high-resolution datasets, will stimulate and guide further theoretical and numerical work in this area.

Future GALFA datasets will clearly find more disk/halo interface clouds and new HVCs, especially in the regime of the smallest HVCs which is largely unexplored. With the larger data sets we will be able to confirm whether the cloudy structure exists at other Galactic longitudes, and also the statistical significance of the potential differences between interface clouds in the inner and outer Galaxy. Also, future GALFA datasets will be important for establishing spatial distribution and properties of the smallest HVCs.

It is a great pleasure to thank all members of the Arecibo Observatory for the successful installation and commissioning of ALFA, as well as their support in undertaking large-scale surveys with this instrument. We would especially like to thank Jeff Hagen and Mikael Lerner for the implementation of the basket-weave scanning mode as a standard data-taking procedure, Arun Venkataraman for numerous network and disk-space related endeavors, Eddie Castro for working very hard on many aspects of the front-end system, and Phil Perillat for crucial details of software development. We would also like to thank Henry Chen for building the GALFA spectrometer. We are indebted to telescope operators for their superb help in running many GALFA projects. The authors are thankful to an anonymous referee for insightful comments that improved the paper. The GALFA Consortium web page is <http://www.naic.edu/alfa/galfa/>. SS and CH acknowledge partial support from NAIC as Visiting Scientists during the period of this work. We acknowledge support by NSF grants AST 04-06987, 00-97417, and 99-81308. J.J.L. was supported by the Korea Science and Engineering Foundation Grant ABRL 3345-20031017. The data cube used in this study is available at <http://astro.berkeley.edu/~sstanimi/Data/>.

REFERENCES

- Albert, C. E. 1983, *ApJ*, 272, 509
 Arnal, E. M., Bajaja, E., Larrarte, J. J., Morras, R., Pöppel, W. G. L. 2000, *A&AS*, 142, 35
 Audit, E. & Hennebelle, P. 2005, *A&A*, 433, 1
 Bajaja, E., Arnal, E. M., Larrarte, J. J., Morras, R., Pöppel, W. G. L., & Kalberla, P. M. W. 2005, *A&A*, 440, 767
 Belfort, P., & Crovisier, J. 1984, *A&A*, 136, 368
 Boissier, S., & Prantzos, N. 1999, *MNRAS*, 307, 857
 Boissier, S., Prantzos, N., Boselli, A., & Gavazzi, G. 2003, *MNRAS*, 346, 1215
 Braun, R., & Burton, W. B. 1999, *A&A*, 341, 437
 Bregman, J. N., Novicki, M. C., Krick, J. E., & Arabadjis, J. S. 2003, *ApJ*, 597, 399
 Brüns, C., Kerp, J., Staveley-Smith, L., Mebold, U., Putman, M. E., Haynes, R. F., Kalberla, P. M. W., Muller, E., & Filipovic, M. D. 2005, *A&A*, 432, 45
 Brüns, C., & Mebold, U. 2004, in *ASSL Vol. 312: High Velocity Clouds*, ed. H. van Woerden, B. P. Wakker, U. J. Schwarz, & K. S. de Boer, 251
 Brüns, C., & Westmeier, T. 2004, *A&A*, 426, L9
 Burton, W. B., Braun, R., & Chengalur, J. N. 2001, *A&A*, 369, 616
 Burton, W. B., & Hartmann, D. 1994, *Ap&SS*, 217, 189
 Collins, J. A., Benjamin, R. A., & Rand, R. J. 2002, *ApJ*, 578, 98
 Cortés-Medellin, G. 2002, Arecibo L-band Feed Array Memo Series, NAIC, Arecibo
 Crawford, I. A., Lallement, R., Price, R. J., Sfeir, D. M., Wakker, B. P., & Welsh, B. Y. 2002, *MNRAS*, 337, 720
 Crochiere, R. E., & Rabiner, L. R. 1983, *Multirate Digital Signal Processing* (Englewood Cliffs, N.J.: Prentice-Hall)
 Danly, L. 1989, *ApJ*, 342, 785
 de Avillez, M. A. 2000, *MNRAS*, 315, 479
 de Heij, V., Braun, R., & Burton, W. B. 2002, *A&A*, 392, 417
 de Heij, V., Braun, R., & Burton, W. B. 2002, *A&A*, 391, 67
 Dickey, J. M. 2002, in *ASP Conf. Ser. 278: Single-Dish Radio Astronomy: Techniques and Applications*, 209
 Dove, J. B., Shull, J. M., & Ferrara, A. 2000, *ApJ*, 531, 846
 Field, G. B., Goldsmith, D. W., & Habing, H. J. 1969, *ApJ*, 155, L149
 Fraternali, F., van Moorsel, G., Sancisi, R., & Oosterloo, T. 2002, *AJ*, 123, 3124

- Hartmann, D., & Burton, W. B. 1997, *Atlas of Galactic Neutral Hydrogen* (Atlas of Galactic Neutral Hydrogen, by Dap Hartmann and W. Butler Burton, pp. 243. ISBN 0521471117. Cambridge, UK: Cambridge University Press, February 1997.)
- Haslam, C. G. T., Stoffel, H., Salter, C. J., & Wilson, W. E. 1982, *A&AS*, 47, 1
- Heiles, C. 1984, *ApJS*, 55, 585
- Heiles, C., & Troland, T. H. 2003a, *ApJS*, 145, 329
- . 2003b, *ApJ*, 586, 1067
- Hoffman, G. L., Salpeter, E. E., & Hirani, A. 2004, *AJ*, 128, 2932
- Houck, J. C., & Bregman, J. N. 1990, *ApJ*, 352, 506
- Howk, J. C. 2005, in *ASP Conf. Ser. 331: Extra-Planar Gas*, 287–+
- Kalberla, P. M. W., Burton, W. B., Hartmann, D., Arnal, E. M., Bajaja, E., Morras, R., & Pöppel, W. G. L. 2005a, *A&A*, 440, 775
- Kalberla, P. M. W., Dedes, L., Arnal, E. M., Bajaja, E., Morras, R., & Pöppel, W. G. L. 2005b, in *ASP Conf. Ser. 331: Extra-Planar Gas*, 81
- Kaufmann, T., Mayer, L., Wadsley, J., Stadel, J., & Moore, B. 2006, *MNRAS*, 370, 1612
- Kolpak, M. A., Jackson, J. M., Bania, T. M., & Dickey, J. M. 2002, *ApJ*, 578, 868
- Koo, B.-C., Kang, J.-h., & Salter, C. J. 2006, *ApJ*, 643, L49
- Kulkarni, S. R., & Heiles, C. 1988, in *Galactic and Extragalactic Radio Astronomy*, ed. K. Kellermann & G. L. Verschur (New York: Springer-Verlag), 95
- Kulkarni, S. R., Heiles, C., & Dickey, J. M. 1985, *ApJ*, 291, 716
- Lindblad, P. O. 1967, *Bull. Astron. Inst. Netherlands*, 19, 34
- Lockman, F. J. 1986, *Gaseous halos of Galaxies*, 63
- Lockman, F. J. 2002, *ApJ*, 580, L47
- Lockman, F. J. 2004, in *Soft X-ray Emission from Clusters of Galaxies and Related Phenomena*, ed. R. Lieu & J. Mittaz (Kluwer Academic Publishers, Dordrecht, The Netherlands), 111
- Lockman, F. J., & Pidopryhora, Y. 2004, in *Extra-planar Gas*, ed. R. Braun, *ASP Conference Series* (ASP, San Francisco)
- Maller, A. H., & Bullock, J. S. 2004, *MNRAS*, 355, 694
- Maloney, P. R., & Putman, M. E. 2003, *ApJ*, 589, 270
- McClure-Griffiths, N. M., Dickey, J. M., Gaensler, B. M., Green, A. J., Haverkorn, M., & Strasser, S. 2005, *ApJS*, 158, 178
- McClure-Griffiths, N. M., Ford, A., Pisano, D., Gibson, B. K., Staveley-Smith, L., Calabretta, M. R., Dedes, L., & Kalberla, P. M. W. 2006, *ApJ*, 638, 196
- Mac Low, M.-M., Balsara, D. S., Kim, J., & de Avillez, M. A. 2005, *ApJ*, 626, 864
- McKee, C. F., & Cowie, L. L. 1977, *ApJ*, 215, 213
- Murali, C., Katz, N., Hernquist, L., Weinberg, D. H., & Davé, R. 2002, *ApJ*, 571, 1
- Murray, S. D., & Lin, D. N. C. 2004, *ApJ*, 615, 586
- Norman, C. A., & Ikeuchi, S. 1989, *ApJ*, 345, 372
- Oort, J. H. 1966, *Bull. Astron. Inst. Netherlands*, 18, 421
- Putman, M. E., de Heij, V., Staveley-Smith, L., Braun, R., Freeman, K. C., Gibson, B. K., Burton, W. B., Barnes, D. G., Banks, G. D., Bhathal, R., de Blok, W. J. G., Boyce, P. J., Disney, M. J., Drinkwater, M. J., Ekers, R. D., Henning, P. A., Jerjen, H., Kilborn, V. A., Knezek, P. M., Koribalski, B., Malin, D. F., Marquarding, M., Minchin, R. F., Mould, J. R., Oosterloo, T., Price, R. M., Ryder, S. D., Sadler, E. M., Stewart, I., Stootman, F., Webster, R. L., & Wright, A. E. 2002, *AJ*, 123, 873
- Putman, M. E., Staveley-Smith, L., Freeman, K. C., Gibson, B. K., & Barnes, D. G. 2003, *ApJ*, 586, 170
- Richter, P., Sembach, K. R., & Howk, J. C. 2003, *A&A*, 405, 1013
- Richter, P., Westmeier, T., & Brüns, C. 2005, *A&A*, 442, L49
- Romney, J. D. 1995, in *ASP Conf. Ser. 82: Very Long Baseline Interferometry and the VLBA*, ed. J. A. Zensus, P. J. Diamond, & P. J. Napier, 17
- Shane, W. W. 1967, *IAU Symp. 31: Radio Astronomy and the Galactic System*, 31, 177
- Shapiro, P. R., & Field, G. B. 1976, *ApJ*, 205, 762
- Stark, A. A., Gammie, C. F., Wilson, R. W., Bally, J., Linke, R. A., Heiles, C., & Hurwitz, M. 1992, *ApJS*, 79, 77
- Stil, J. M., Lockman, F. J., Taylor, A. R., Dickey, J. M., Kavars, D. W., Martin, P. G., Rothwell, T. A., Boothroyd, A., & McClure-Griffiths, N. M. 2006, *ApJ*, 637, 366
- Tamanaha, C. M. 1994, *ApJ*, 433, 648
- . 1997, *ApJS*, 109, 139
- Taylor, A. R., Gibson, S. J., Peracaula, M., Martin, P. G., Landecker, T. L., Brunt, C. M., Dewdney, P. E., Dougherty, S. M., Gray, A. D., Higgs, L. A., Kerton, C. R., Knee, L. B. G., Kothes, R., Purton, C. R., Uyaniker, B., Wallace, B. J., Willis, A. G., & Durand, D. 2003, *AJ*, 125, 3145
- Wakker, B. P. 2001, *ApJS*, 136, 463
- Wakker, B. P., Savage, B. D., Sembach, K. R., Richter, P., Meade, M., Jenkins, E. B., Shull, J. M., Ake, T. B., Blair, W. P., Dixon, W. V., Friedman, S. D., Green, J. C., Green, R. F., Kruk, J. W., Moos, H. W., Murphy, E. M., Oegerle, W. R., Sahnou, D. J., Sonneborn, G., Wilkinson, E., & York, D. G. 2003, *ApJS*, 146, 1
- Wakker, B. P., & van Woerden, H. 1991, *A&A*, 250, 509
- Weaver, H. F. 1970, *IAU Symp. 39: Interstellar Gas Dynamics*, 39, 22
- Wolfire, M. G., McKee, C. F., Hollenbach, D., & Tielens, A. G. G. M. 1995, *ApJ*, 453, 673
- Wolfire, M. G., McKee, C. F., Hollenbach, D., & Tielens, A. G. G. M. 2003, *ApJ*, 587, 278